Charging and trapping of macroparticles in near-electrode regions of fluorocarbon plasmas with negative ions

K. N. Ostrikov, S. Kumar, and H. Sugai

Citation: Physics of Plasmas (1994-present) **8**, 3490 (2001); doi: 10.1063/1.1375149
View online: http://dx.doi.org/10.1063/1.1375149
View Table of Contents: http://scitation.aip.org/content/aip/journal/pop/8/7?ver=pdfcov
Published by the AIP Publishing

Charging and trapping of macroparticles in near-electrode regions of fluorocarbon plasmas with negative ions

K. N. Ostrikov[a)]
Department of Electrical Engineering, Nagoya University, Furo-cho, Chikusa-ku, Nagoya 464-8603, Japan; Plasma Processing Laboratory, NIE, Nanyang Technological University, 1 Nanyang Walk, 637616 Singapore;
and School of Chemistry, Physics, and Earth Sciences, The Flinders University of South Australia, GPO Box 2100, Adelaide SA 5001, Australia

S. Kumar
Ian Wark Research Institute, The University of South Australia, Mawson Lakes SA 5095, Australia

H. Sugai
Department of Electrical Engineering, Nagoya University, Furo-cho, Chikusa-ku, Nagoya 464-8603, Japan

(Received 7 February 2001; accepted 23 March 2001)

Charging and trapping of macroparticles in the near-electrode region of fluorocarbon etching plasmas with negative ions is considered. The equilibrium charge and forces on particles are computed as a function of the local position in the plasma presheath and sheath. The ionic composition of the plasma corresponds to the etching experiments in 2.45 GHz surface-wave sustained and 13.56 MHz inductively coupled C_4F_8+Ar plasmas. It is shown that despite negligible negative ion currents collected by the particles, the negative fluorine ions affect the charging and trapping of particulates through modification of the sheath/presheath structure. © *2001 American Institute of Physics.* [DOI: 10.1063/1.1375149]

I. INTRODUCTION

Modern technologies for fabrication of the new generation ultra-large-scale integrated circuits require high selectivity and rate of the etching process. The etching parameters and quality strongly depend on the feedstock gas composition and the kind of gas discharge used.[1] Indeed, the dominating power and particle transport mechanisms in a discharge control the chemistry of active species. In particular, it has been recently revealed that inductively coupled (IC) and surface wave sustained (SWS) plasmas produced in C_4F_8+Ar gas mixtures have an outstanding potential for ultra-fine and highly selective etching of large-area polysilicon wafers.[2,3] Physically, it appears possible to achieve high dissociation rates of the feedstock gas and densities ($\sim 10^{13}\,cm^{-3}$) of neutral radicals at low ($\sim$20 mTorr) pressures.

However, fluorine atoms and other fluorocarbon radicals relatively easily become negatively charged, in particular, due to electron attachment. Recent data on laser photodetachment measurements in high-density C_4F_8+Ar plasmas suggest that under certain conditions negative ions can constitute a substantial proportion among other discharge species.[4] Negative ions modify the power and particle transport, and the potential distribution in the discharge. Furthermore, in pulsed discharges, negative ions can directly participate in the substrate etching process.

Negative charge can also be carried by macroparticles, which are created as a result of the gas-phase polymerization[5] or release of the underlying substrate or deposited film material into the plasma.[6] The size of particles is typically in a micron range, and any sizes from hundreds of nanometers to tens of microns have been reported so far.[7,8] Thus, the fallout of such particles onto a wafer with a 0.1 μm design rule can produce unrecoverable defects. Hence, the problem of trapping and removal of macroparticles from the processing volume becomes crucial.[9] The key parameter that controls the particle trapping process is the electrical charge, which is usually negative due to efficient collection of highly mobile plasma electrons. The equilibrium charge on a particle is determined by a balance between positive and negative microscopic currents.[10,11]

Furthermore, it has recently been demonstrated that in the bulk of C_4F_8+Ar inductively coupled and surface wave sustained plasmas positive fluorocarbon ions can significantly affect the macroparticle charging and charge relaxation processes.[12] In this article, we consider the effect of negative ions on particulate charging and trapping in the near-electrode region of fluorocarbon plasmas. We assume that the charge proportion on negatively charged dusts is low, and the particulates do not affect the structure of the sheath/presheath region.

On the other hand, we investigate how a substantial proportion of negative fluorine ions affects the structure and electron/ion number density distribution in the near-electrode region. The effect of the sheath composition and structure on the average dust charge is also studied taking into account the dependence of the electron/ion number densities and hydrodynamic velocities on a local position in the near-

[a)]Also at Department of Electrical and Electronic Engineering, Nanyang Technological University, 639798, Singapore. Electronic mail: ekostrikov@ntu.edu.sg and Kostya.Ostrikov@flinders.edu.au

electrode region. It is demonstrated that the effect of negative ions is most feasible in the electronegative presheath, where the particulate charge appears to be lower than in negative-ion-free plasmas. It is also revealed that the dynamics of the particulates in the near-electrode area of high-density C_4F_8+Ar plasmas is mainly controlled by a competition between the electrostatic force and the positive ion drag force, the latter including contributions from Ar^+, CF^+, CF_2^+, and CF_3^+ ions. It appears possible to trap 0.3 and 2 μm sized particles at the position, fairly corresponding to the sheath edge.

The article is organized as follows. In Sec. II, the problem is formulated and the basic assumptions are given. The model of the near-wall region of C_4F_8+Ar plasmas with negative ions is formulated and the spatial profiles of the electron/ion number density are computed in Sec. III. Section IV is devoted to calculation of the equilibrium charge on the particles as a function of local position with respect to the electrode. In Sec. V, the forces acting on the particles in the plasma bulk, and the sheath/presheath regions are computed. The key effects of negative ions on particulate charging and trapping in fluorocarbon plasmas are highlighted in Sec. VI. The results are briefly summarized in Sec. VII.

II. FORMULATION

In our model, the one-dimensional configuration, with an electrode placed at $x=0$, is adopted. The plasma occupies the region $x>0$. The structure is assumed infinite in the y and z directions. The width of the near-electrode region, which is normally referred to as a combined thickness of the sheath and presheath, is x_{ps}. The region $x>x_{ps}$ (plasma bulk) is occupied by the uniform plasma. However, within the region $x<x_{ps}$, all variables are functions of distance x from the electrode.

It is assumed that the plasma is composed of electrons, positive Ar^+, CF^+, CF_2^+, and CF_3^+, as well as negative F^- ions, which is representative of experiments on highly selective poly-silicon etching in gas mixtures of octafluorocyclobutane ($c-C_4F_8$) and argon.[2,3,13–16] The overall charge neutrality

$$n_e+n_{F^-}+n_d|Z_d|=n_{Ar^+}+n_{CF^+}+n_{CF_2^+}+n_{CF_3^+}$$

holds in a plasma bulk. Here, $n_{(j)}$ is a number density of the plasma species ($j=e$, F^-, d, Ar^+, CF^+, CF_2^+, and CF_3^+), and Z_d is the average charge on a particulate. However, we assume that the charge number density of negative dusts is low, so that $n_d|Z_d|\ll n_e+n_{F^-}$. Hence, the particulates do not affect the structure of the plasma either in the bulk or near the electrode. The specific plasma parameters and proportions of positive ions have been taken as typical values from the experiments on SiO_2 wafer etching in 2.45 GHz SWS and 13.56 MHz IC plasmas at low pressures.[3] In particular, in 90% Ar and 10% C_4F_8 gas mixture at 20 mTorr, proportion of argon ions varies from 55% in the surface wave plasmas sustained with ~400 W to about 90% in the ICP (~1.5 kW).[3] Both plasmas feature dominant CF^+, CF_2^+, and CF_3^+ fluorocarbon ion radicals in a wide range of RF input powers. The positive ion number densities satisfy $n_{CF^+}>n_{CF_2^+}>n_{CF_3^+}$, whereas that of other ions, such as $C_xF_y^+$, $x>1$, C_x^+, and F^+, appear to be much lower.

Due to the lack of simultaneously measured data on positive and negative ionic composition in electronegative C_4F_8+Ar discharges, we assume that proportion of negative ions varies within 15% and 45% from the total number density of negative charge, which falls within the typical values of the combined charge carried by negative ions.[4,16]

III. MODEL OF THE NEAR-WALL REGION

Due to overwhelming complexity of gas-phase reactions and large number of elementary processes in the fluorocarbon plasmas with negative ions, the fully self-consisted description of the near-electrode region seems rather complicated and some simpler model is to be used instead. We recall that in conventional sheath models the equilibrium potential profile is derived from the set of particle balance equations for ionic species and Poisson's equation.[17] Here, we do not aim at considering power and particle balance processes in the discharge and need to make a realistic choice of the near-wall potential $\phi(x)$, and then compute the density profiles within the sheath/presheath, consistent with Poisson's equation

$$\frac{d^2\phi(x)}{dx^2}=4\pi e[n_e(x)+n_{F^-}(x)-n_{Ar^+}(x)-n_{CF^+}(x)-n_{CF_2^+}(x)-n_{CF_3^+}(x)], \tag{1}$$

where we have assumed the electrons and negative ions to be Boltzmann distributed,

$$n_e(x)=n_0(1-\alpha_{F^-})\exp[e\phi(x)/T_e], \tag{2}$$

$$n_{F^-}(x)=n_0\alpha_{F^-}\exp[e\phi(x)/T_{F^-}], \tag{3}$$

and e is the electron charge, T_e and T_{F^-} are the temperatures of electrons and negative fluorine ions. Here,

$$n_0=n_e(x_{ps})+n_{F^-}(x_{ps})=n_{Ar^+}(x_{ps})+n_{CF^+}(x_{ps})+n_{CF_2^+}(x_{ps})+n_{CF_3^+}(x_{ps})$$

is the combined number density of negative or positive plasma species in the plasma bulk ($x=x_{ps}$), and $\alpha_{F^-}=n_{F^-}(x_{ps})/n_0$.

The overall charge neutrality in the plasma bulk and Eq. (1) dictate that $d^2\phi(x_{ps})/dx^2=0$. Furthermore, assuming the plasma potential and electric field vanish in the plasma bulk, we have $d\phi(x_{ps})/dx=0$ and $\phi(x_{ps})=0$, respectively. The sheath potential, which satisfies all the above requirements and produces almost linear dependence of the electrostatic field on the local position x, is depicted in Fig. 1, where $\phi_0\equiv\phi(0)=-5$ V. Similar potential distributions have been recently reported in the experiments on the effect of micron-size dusts on sheath structure of the low-pressure hot filament discharge.[18] We have further assumed that the relative proportions of fluorocarbon positive ions $\alpha_{CF^+}:\alpha_{CF_2^+}:\alpha_{CF_3^+}$

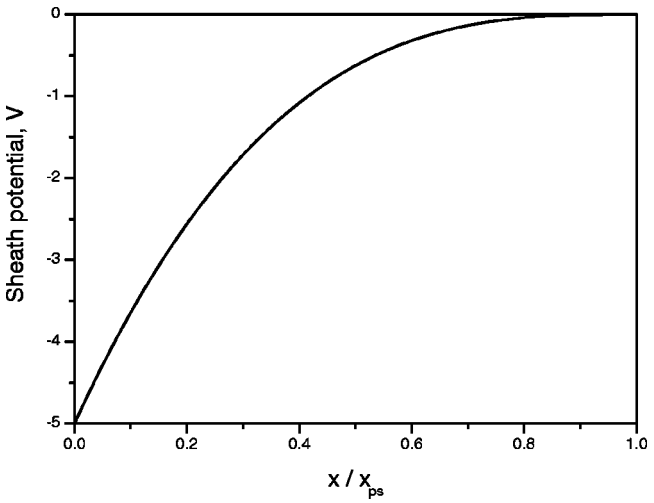

FIG. 1. Model potential profile in the near-electrode region.

TABLE I. The main plasma and particulate parameters in the computation.

Parameter	Notation	Value
Electron temperature	T_e	2.0 eV
Particulate size	a	0.3, 2.0 μm
Particulate mass density	ρ	1.5 g/cm^3
Plasma bulk density	n_0	4×10^{11} cm^{-3}
Ion mass (Ar^+)	m_{Ar^+}	$1836\times40\times m_e$
Ion mass (F^-)	m_{F^-}	$1836\times19\times m_e$
Ion mass (CF^+)	m_{CF^+}	$1836\times31\times m_e$
Ion mass (CF_2^+)	$m_{CF_2^+}$	$1836\times50\times m_e$
Ion mass (CF_3^+)	$m_{CF_3^+}$	$1836\times69\times m_e$
Ion temperature (all ions)	$T_{(j)}$	0.067 eV
Temperature of neutrals	T_n	0.026 eV
Electrode potential	ϕ_0	-5.0 V
Ion proportion (Ar^+)	α_{Ar^+}	0.55–0.95
Ion proportion (F^-)	α_{F^-}	0.15–0.45
Ion proportion (CF^+)	α_{CF^+}	$(1-\alpha_{Ar^+})\times0.5$
Ion proportion (CF_2^+)	$\alpha_{CF_2^+}$	$(1-\alpha_{Ar^+})\times0.3$
Ion proportion (CF_3^+)	$\alpha_{CF_3^+}$	$(1-\alpha_{Ar^+})\times0.2$

do not vary with x, so the temperatures of the plasma particles do not, where $\alpha_{(j)}=n_{(j)}(x_{ps})/n_0$, and j stands for any of the positive ionic species.

We now turn to description of ion motion in the near-electrode region. It should be noted that in the experiments of our interest the plasma sheath is RF-driven, and the key parameter to be taken into account is the ratio of the ion sheath traverse time τ_{sh} to the period of the RF field T_{RF}. Here, we consider the case when $T_{RF}\ll\tau_{sh}$ and, hence, the ions respond to the time-averaged (over the time scales $\tau_{sh}\sim t\gg T_{RF}$) electric field.[19]

The positive ion fluid velocities $v_{(j)f}$ satisfy the following momentum equation,

$$v_{(j)f}\frac{dv_{(j)f}}{dx}+\nu_{(j)n}v_{(j)f}=-\frac{e}{m_{(j)}}\frac{d\phi(z)}{dx}, \tag{4}$$

where $\nu_{(j)n}=N_n\sigma_{(j)n}v_{(j)}$ is the rate of the ion-neutral collisions, N_n is the density of neutrals, $v_{(j)}=[v_{(j)f}+8T_{(j)}/\pi m_{(j)}]^{1/2}$, and $m_{(j)}$ and $T_{(j)}$ are the ion mass and temperature, respectively. We note that the ion-neutral collision cross-section $\sigma_{(j)n}$ is a function of the ion velocity, the latter varying in the sheath/presheath region. For $\sigma_{(j)n}$, we have

$$\sigma_{(j)n}(v_{(j)})[10^{-14}\,\mathrm{cm}^2]=\frac{0.06}{\mathcal{E}_{(j)}}\left[\ln\left(\frac{6\times10^9\sqrt{\mathcal{E}_{(j)}}}{v_{(j)}}\right)\right]^2, \tag{5}$$

which accurately approximates the cross section for resonance charge exchange for argon, and yields an error less than 50% for a number of another ionic species,[20] where $\mathcal{E}_{(j)}$ is the ion energy in electron-volts.

The parameters of the plasma and macroparticles used in the computation are summarized in Table I. Using the data of Table I, and Eqs. (1)–(5), the profiles of the number densities of all plasma species have been computed (Figs. 2 and 3). Figure 2 displays how distribution of the electron/ion number densities in the near-electrode region varies with argon content α_{Ar^+}. Figure 2(a), with lower ($\alpha_{Ar^+}=0.55$) argon ion content, corresponds to the low-power surface wave sustained plasmas, while Fig. 2(c) ($\alpha_{Ar^+}=0.95$) stands for

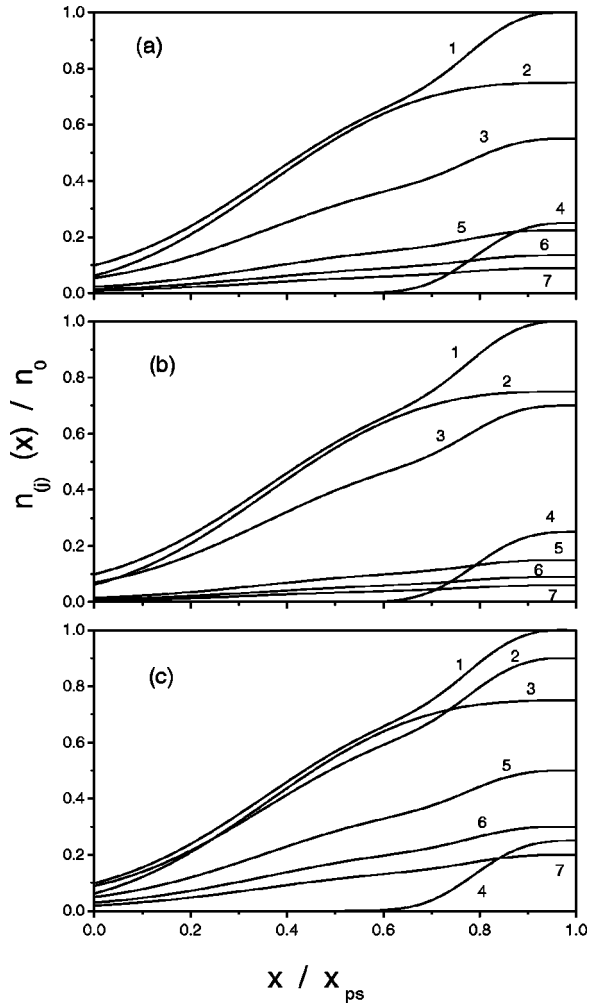

FIG. 2. Profiles of nondimensional (normalized on n_0) number densities of charged species for $\alpha_{F^-}=0.25$ and $\alpha_{Ar^+}=0.55$ (a), 0.7 (b), and 0.95 (c), respectively. Other parameters are given in Table I. Curves 1–7 correspond to $\Sigma_{(j^+)}n_{(j^+)}$, n_e, Ar^+, F^-, CF^+, CF_2^+, and CF_3^+, respectively. In diagram (c), number densities of CF^+, CF_2^+, and CF_3^+ are multiplied by a factor of 10.

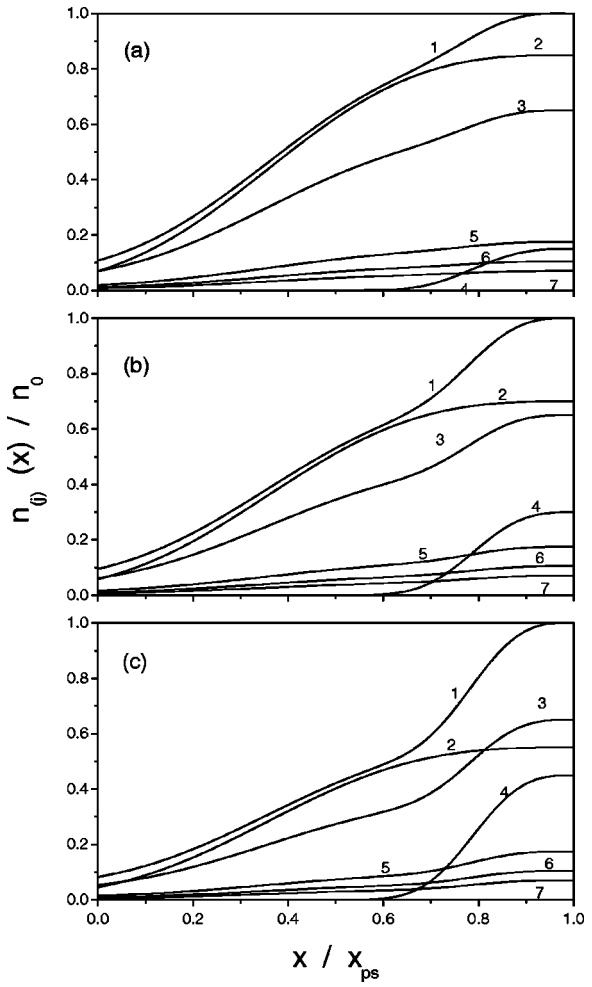

FIG. 3. Same as in Fig. 1 for $\alpha_{Ar^+}=0.65$ and $\alpha_{F^-}=0.15$ (a), 0.3 (b), and 0.45 (c), respectively.

higher-power inductively coupled plasmas.[3] Figure 3 reflects the change in the sheath/presheath composition with variation of the number density of negative fluorine atoms. In particular, from Fig. 3(c) one can see that if the number density of negative ions is large enough, the electron density can be depleted and become less than that for positive argon ions.

From Figs. 2 and 3 we see that the number density of negative ions dramatically decreases towards $x\sim 0.6x_{ps}$, and is negligible in the area closer to the electrode. Furthermore, the computation suggests that all ion velocities $v_{(j)}$, being equal to the ion thermal velocity $V_{T(j)}=\sqrt{8T_{(j)}/\pi m_{(j)}}$ in the plasma bulk, become equal to the ion-acoustic velocity $V_{S(j)}=\sqrt{T_e/m_{(j)}}$ within the area $0.2<x/x_{ps}<0.3$. Thus, it sounds reasonable to tentatively call the area $0.6<x/x_{ps}<1$ as the electronegative region, or the presheath with negative ions (region I), $x_s<x/x_{ps}<0.6$ as the electropositive region, or the presheath without negative ions (region II), and $0<x/x_{ps}<x_s$ as a sheath itself (region III). The uncertainty in the sheath edge location x_s falls within the limits $0.2x_{ps}<x_s<0.3x_{ps}$. The exact location of the sheath edge can be obtained by applying the Bohm sheath criterion for multicomponent plasma.[21] In region I, positive ions are accelerated towards the electrode, and negative ions contribute to the sheath structure. In region II, ions are further accelerated, whereas the effect of negative ions to the sheath structure is already negligible. In the near-wall region III, the electron and ion densities diminish, the latter remains higher sustaining the electrostatic field in the sheath. Our approximate model thus reflects basic features of plasma sheaths in electronegative gases.[22]

IV. PARTICULATE CHARGING

The value of the average particulate charge is determined by the dynamic charging equation

$$\frac{dq_d}{dt}=\Sigma_{(j^-)}I_{(j^-)}(q_d,x)+\Sigma_{(j^+)}I_{(j^+)}(q_d,x), \tag{6}$$

where $q_d=-|Z_d|e$ is a negative dust charge, and $\Sigma_{[j(+,-)]}I_{[j(+,-)]}(q_d,x)$ are the combined microscopic currents of positive and negative plasma species, and

$$\Sigma_{(j^-)}I_{(j^-)}(q_d,x)=I_e(q_d,x)+I_{F^-}(q_d,x),$$

$$\Sigma_{(j^+)}I_{(j^+)}(q_d,x)=I_{(Ar^+)}(q_d,x)+I_{CF^+}(q_d,x)+I_{CF_2^+}(q_d,x)+I_{CF_3^+}(q_d,x),$$

and we notice that the grain currents are the functions of the local position with respect to the electrode.

The microscopic currents onto the dust grain in the orbit motion limited (OML) approximation are[23,24]

$$I_e(q_d,x)=-\pi a^2 e(8T_e/\pi m_e)^{1/2}n_e(x)\exp[e\,\delta\phi_d(x)/T_e], \tag{7}$$

$$I_{F^-}(q_d,x)=-\pi a^2 e v_{F^-}(x)n_{F^-}(x)\exp[e\,\delta\phi_d(x)/T_{F^-}], \tag{8}$$

and

$$I_{(j^+)}(q_d,x)=\pi a^2 e v_{(j^+)}(x)n_{(j^+)}(x)\times[1-2e\,\delta\phi_d/m_{(j^+)}(v_{(j^+)}(x))^2], \tag{9}$$

where $\delta\phi_d=-e|Z_d|/a$ is the potential drop between a spherical macroparticle with an average radius a and the adjacent plasma.

In the equilibrium state ($q_{d0}=$const), the microscopic currents of positive and negative plasma particles balance each other, so that

$$\Sigma_{(j^-)}I_{(j^-)}(q_{d0},x)+\Sigma_{(j^+)}I_{(j^+)}(q_{d0},x)=0,$$

which, after normalization, yields the following transcendental equation for the equilibrium dust charge Z_{d0}

$$B_e+B_{F^-}-B_{Ar^+}-B_{CF^+}-B_{CF_2^+}-B_{CF_3^+}=0, \tag{10}$$

where

$$B_e=\delta_e(x)\exp[-\Theta(x)],$$

$$B_{F^-}=(\xi_{F^-}/\mu_{F^-})^{1/2}\delta_{F^-}(x)\exp[-\Theta(x)/\tau_{F^-}],$$

and

$$B_{j^+}=[\xi_{(j^+)}/\mu_{(j^+)}]^{1/2}\delta_{(j^+)}(x)[1+\varrho\Theta(x)/\xi_{(j^+)}],$$

where $\delta_{(j)}(x)=n_{(j)}(x)/n_0$, $\xi_{(j)}=\varrho\zeta_{(j)}^2(x)/2+\tau_{(j)}$, $\tau_{(j)}=T_{(j)}/T_e$, $\zeta_{(j)}=v_{(j)}/v_{S(j)}$, $\mu_{(j)}=m_{(j)}/m_e$, $\Theta=e^2|Z_d|/aT_e$, and $\varrho=\pi/4$.

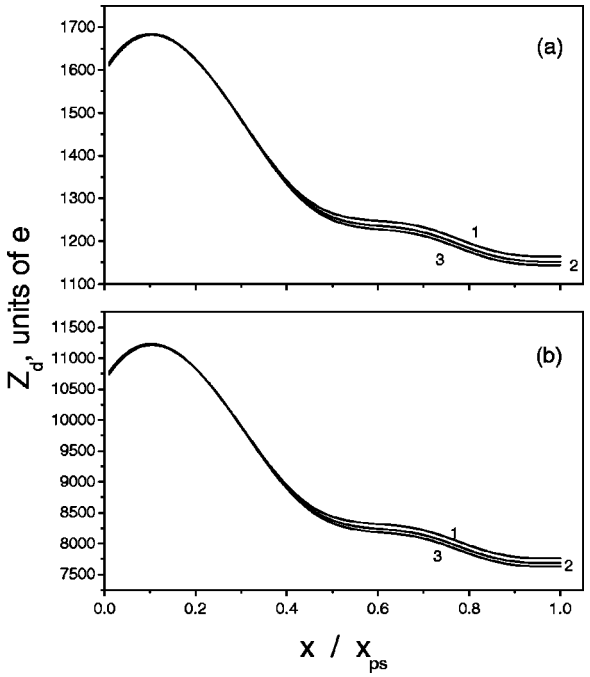

FIG. 4. Profiles of the equilibrium charge $Z_{d0}(x)$ on 0.3 (a) and 2 μm (b) particulates in the near-electrode region for $\alpha_{F^-}=0.25$. Other parameters are given in Table I. Curves 1–3 correspond to $\alpha_{Ar^+}=0.9$ (a), 0.7 (b), and 0.55 (c), respectively.

Equations (10), (4), (5), and (1), have been solved numerically to yield the spatial profiles of the equilibrium particulate charge depicted in Figs. 4 and 5, for 0.3 and 2 μm macroparticles, respectively.

Figures 4 and 5 reveal that the particulate charge has a tendency to grow in the near-wall region, and starts to decline after reaching maximum at $x\sim 0.12x_{ps}$. Likewise, the dependence $Z_{d0}(x)$ features distinctive minimum in the electronegative region, which reflects the dust charge depletion caused by negative ions. If the proportion of negative ions is low (curve 1, Fig. 5), the dust charge is almost independent on local position within $0.5x_{ps}<x$. In the region $0.12x_{ps}<x<0.5x_{ps}$ the charge rises, which is a consequence of increasing electron/ion currents onto the grain. Physically, diminishing of the potential lowers the potential barrier for the plasma electrons, which can be more easily collected by the particulates. Meanwhile, strong electron/ion density depletion within the sheath results in declining of microscopic fluxes on dusts and, hence, of $|Z_d|$. Simulations of dust levitation in argon plasma sheaths report similar trends in dependence $Z_d(x)$.[25]

From Fig. 4 one can see that an increase of the argon proportion augments the dust charge in both electronegative and electropositive regions. However, in the sheath region Z_d appears to be almost insensitive to α_{Ar^+}. Furthermore, the particulate charge is lower when the number density of negative fluorine atoms in the electronegative region is higher (Fig. 5). Above all, variation of δ_{F^-} (essentially in region I) appears to affect the particulate charge in the sheath (region III). Physically, negative ions affect formation of ion flows originating in the electronegative region and, hence, the grain currents within the sheath.

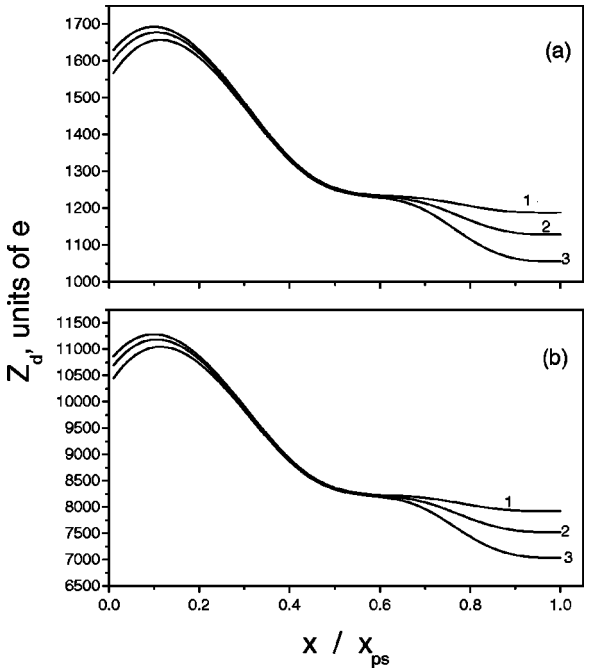

FIG. 5. Same as in Fig. 4 for $\alpha_{Ar^+}=0.65$. Curves 1–3 correspond to $\alpha_{F^-}=0.15$ (a), 0.3 (b), and 0.45 (c), respectively.

V. FORCES ACTING ON PARTICULATES

Knowledge of the ion velocity and dust charge distributions allows one to compute the forces acting on particulates. The latter include the gravity, electrostatic, and ion drag forces[23]

$$F_{\rm tot}(x)=-F_g+|F_{\rm el}(x)|+F_{\rm dr}^{(j^-)}(x)-F_{\rm dr}^{(j^+)}(x), \qquad (11)$$

where $F_g=m_dg$, $F_{\rm el}(x)=q_d(x)E(x)$, and $m_d=(4\pi/3)a^3\rho_d$ and ρ_d are the particulate mass and mass density, respectively. The ion drag force involves the collection force originating from collection of plasma particles by the dusts $F_{\rm dr,coll}^{(j)}(x)$ and the orbit force due to momentum exchange in the course of Coulomb collisions $F_{\rm dr,orb}^{(j)}(x)$. Note that the positive and negative ion drag forces have different directions with respect to the electric force. In the OML approximation, we have[23,24]

$$F_{\rm dr,coll}^{[j^{(+,-)}]}(x)=\pi[b_c^{[j^{(+,-)}]}(x)]^2m_{(j)}n_{(j)}(x)v_{(j)}(x)v_{(j)f}(x), \qquad (12)$$

where

$$b_c^{(j^+)}(x)=a[1+2T_e\Theta(x)/m_{(j^+)}v_{(j^+)}^2]^{1/2}$$

is the collection impact parameter for positive ionic species (Ar^+, CF^+, CF_2^+, and CF_3^+), and

$$b_c^{(F^-)}(x)=a\exp[-2T_e\Theta(x)/m_{F^-}v_{F^-}^2(x)]^{1/2}$$

is that for the negative fluorine ions.

The orbit component of the ion drag force is

$$F_{\rm dr,orb}^{(j)}(x)=4\pi e^4|Z_d(x)|^2\Lambda\frac{n_{(j)}(x)v_{(j)f}(x)}{m_{(j)}v_{(j)}^3(x)}, \qquad (13)$$

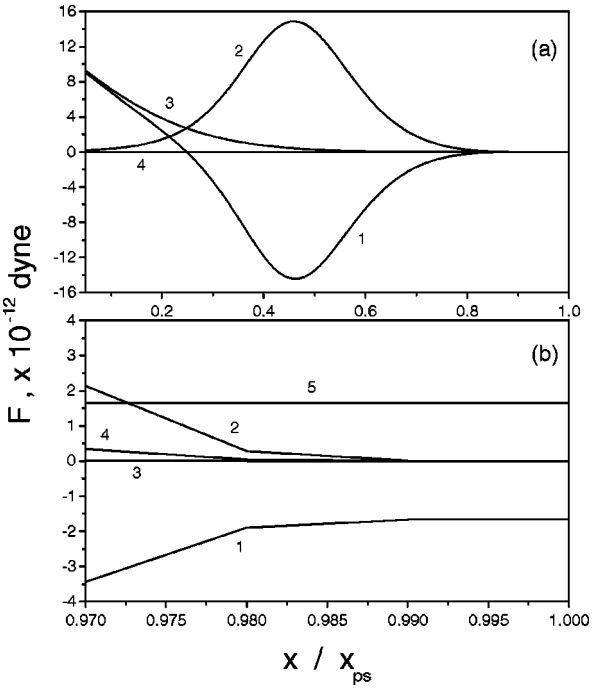

FIG. 6. Forces acting on 0.3 μm particulates in the entire near-electrode region (a) and in the electronegative plasma bulk (b) for $\alpha_{F^-}=0.25$ and $\alpha_{Ar^+}=0.55$. Curves 1–5 correspond to F_{tot}, $F_{dr}^{(j^+)}$, F_{el}, $F_{dr}^{(j^-)}$, and F_g, respectively. Other parameters are given in Table I.

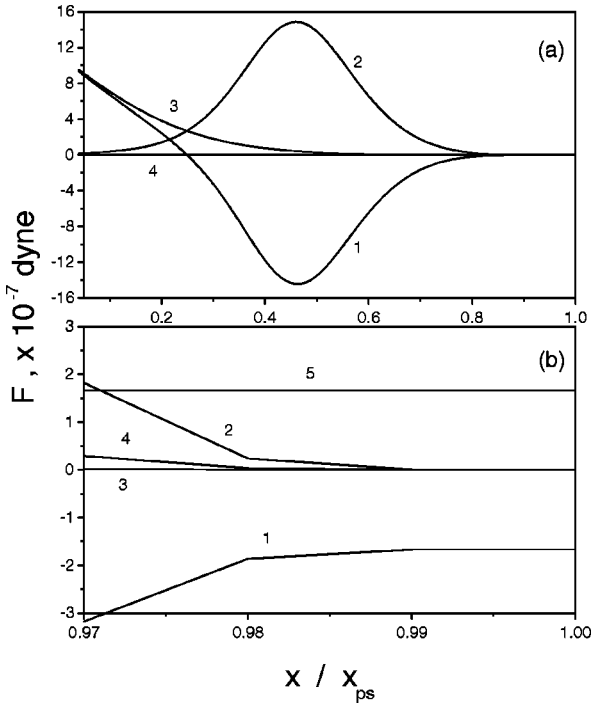

FIG. 7. Same as in Fig. 6 for $\alpha_{F^-}=0.45$ and $\alpha_{Ar^+}=0.65$.

where Λ is the Coulomb logarithm. We note that the forces acting on particulates depend on the local position, and so does the dust charge. This implies that $|Z_d|$ varies instantaneously with x, or, in other words, the dust charge relaxation processes[10,11] are neglected.

The profiles of the forces acting on 0.3 and 2 μm particulates are depicted in Figs. 6–8. Diagrams (a) stand for the entire near-electrode region $0<x<x_{ps}$, while (b) stands for the electronegative one $0.92x_{ps}<x$. Figures 6 and 7 correspond to modest proportions of argon ions ($\alpha_{Ar^+}=0.55$ and 0.65, respectively), which is the case of the SWS C_4F_8+Ar discharge.[3] In Fig. 8, proportion of argon ions is elevated ($\alpha_{Ar^+}=0.75$), which is the case in the ICP discharges with RF powers ~1200–1400 W.[3] It is seen that in nearly the whole electronegative and electropositive presheaths the macroparticles are pushed by the positive ion drag force towards the electrode without any serious counteraction by other forces. In the electronegative region $F_{dr}^{(j+)}(x)$ increases, reaches maximum in region II at $x\sim 0.5x_{ps}$ and declines towards the electrode thereafter. We notice that the flex point in the ion drag force corresponds to the area of significant depletion of the positive ion number density (Figs. 2 and 3). We further infer that the resulting force on particulates F_{tot} is negative (directed towards the electrode) in the entire region $x_{tr}<x$ and reverses at $x\sim x_{tr}$, where $x_{tr}\sim 0.25x_{ps}$ in Figs. 6 and 7, and $x_{tr}\sim 0.18x_{ps}$ in Fig. 8. It is also seen from Figs. 6–8 that the force of gravity makes noticeable contribution only in the plasma bulk [diagrams (b)].

The electrostatic force, negligible in the plasma bulk [curve 2, diagram (b)], becomes comparable with the positive ion drag force at positions $x<0.35x_{ps}$. Inside the sheath (region 3) the force on a particle is essentially electrostatic and pushes it outwards. Indeed, the electric field becomes strong (in our example it is ~200 V/cm in the electrode proximity), while the ion drag force diminishes further. At the equilibrium (particle trapping position[9]) $x=x_{eq}$ the electrostatic and negative ion drag forces balance the positive ion drag force and gravity

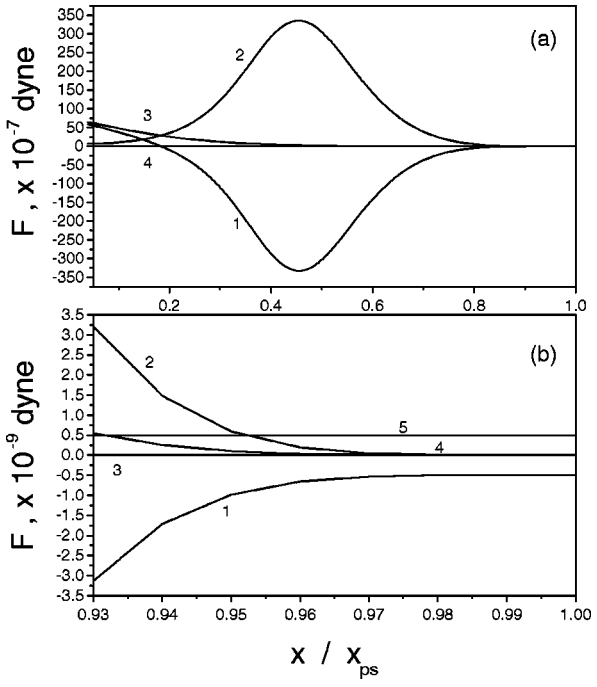

FIG. 8. Same as in Fig. 6 for 2 μm particles, $\alpha_{F^-}=0.25$ and $\alpha_{Ar^+}=0.75$.

$$|F_{\rm el}(x_{\rm eq})| + F_{\rm dr}^{(j^-)}(x_{\rm eq}) = F_{\rm dr}^{(j^+)}(x_{\rm eq}) + F_g\,,$$

and the total force on the particulate vanishes. From Figs. 6 and 7 we note that the particle trapping position is $x_{\rm eq} \sim 0.25 x_{ps}$. As evidenced by Fig. 8, the equilibrium position of the larger (2 μm) particle appears to be closer to the electrode ($x_{\rm eq} \sim 0.18 x_{ps}$). We note that this is consistent with the experimental results on dust void formation.[26] One can thus presume that the effect of positive ion drag force is stronger for larger particles. It is worthwhile to mention that in the near electrode regions of low-density ($\sim 10^9$ cm^{-3}) hot cathode discharges the effect of the ion drag force on micron size dust grains is negligible.[18]

VI. DISCUSSION

We now discuss the main features and implications of micron- and submicron-size particulate charging and trapping in the near-electrode area of the fluorocarbon plasma with negative ions. We emphasize that due to the negative dust potential, the collection impact parameter, and hence the microscopic grain current of negative fluorine atoms, appear to be small. Hence, the major effect of negative ions on the equilibrium particulate charge is associated with the electron density depletion in the electronegative region I (Figs. 2 and 3). Indeed, in the plasma bulk/electronegative pre-sheath, Z_d is 10%–30% lower than in the absence of fluorine ions (Figs. 4 and 5).

It is instructive to note that due to repulsion by the negative sheath potential, fluorine ions do not affect the structure of the sheath (region III). In our example, $n_{\rm F^-}$ sharply declines in the vicinity of $x \sim 0.6 x_{ps}$ (Figs. 2 and 3). Meanwhile, in the region $0.2 < x/x_{ps} < 0.6$, where the number density of negative ions is negligible, dust charge raises dramatically (Figs. 4 and 5). Indeed, assuming that the electron grain current is quasi-continuous at the edge between the electronegative and electropositive regions ($x \sim 0.6 x_{ps}$), from Eq. (10) it follows that Z_d increases. Further rise in the particulate charge can be attributed to the enhancement of the electron/ion grain currents in the spatially varying potential.[25]

Likewise, negative ions are not expected to affect the particulate trapping in region III. However, as Fig. 5 suggests, the dust charge within a sheath is a function of fluorine ion number density in the plasma bulk. Physically, this can be regarded as an example of action of the ''pre-history'' effects associated with formation and acceleration of ion flows in the electronegative presheath region.

The grain size appears to be a factor in determining the equilibrium position of the particulates in the near-electrode region. In particular, we have shown that the trapping point of 2 μm sized particles is closer to the electrode than that for 0.3 μm dusts. Hence, extra care should be taken to prevent the fallout of bigger particles onto the electrode.

Meanwhile, it becomes apparent that in high-density fluorocarbon plasmas the negative ion drag force is weak, and so is the gravity. Furthermore, the orbit component dominates in the positive ion drag force. The gravity effects for both 0.3 and 2 μm particles appear to be important in the plasma bulk only. Within the region $x < 0.9$, the competition between the positive ion drag and electrostatic forces controls the particulate dynamics. The ion drag force peaks at $x \sim 0.45 x_{ps}$, which reflects the dynamic balance between the counteracting effects of positive ion acceleration towards the electrode and depletion of their number density in regions II and III.

In the above, it has been remarked that the accuracy of description of the ion dynamics depends on the relation between the ion sheath traverse time and the RF frequency. For the parameters of Figs. 6 and 7, the argon ion sheath traverse time is $\tau_{\rm sh}^{\rm Ar^+} \sim 3.32 \times 10^{-7}$ s, which is much larger than the period of the conventional 13.56 RF field $T_{\rm RF}$. The sheath traverse time for other ions turns out to be somehow larger. Hence, in our model the ions indeed respond to the time-averaged field and Eq. (4) is correct. However, should the sheath be driven by lower-frequency ($\sim$500 kHz) RF fields,[27] the inequality $\tau_{\rm sh} \ll T_{\rm RF}$ can eventually become incorrect.

It is remarkable that there is controversy in the knowledge of the ion/radical composition of electronegative fluorocarbon plasmas and the available to date experimental data are far from being complete. Furthermore, the overwhelming complexity of fluorocarbon chemistry does not allow us to specify the exact composition of active species. For this reason, it has been assumed that negative ions in the model fluorocarbon discharge are solely represented by negative fluorine ions.

Recent electron photodetachment measurements evidence that in C_4F_8+Ar gas mixtures the integral number density of fluorine negative ions can be comparable with the electron density.[4] We believe that the experiments and self-consistent modeling of the composition of fluorocarbon plasmas should be continued to provide reliable data on $\alpha_{\rm F^-}$.

Our simulation of the near-electrode region, although based on the preset function $\phi(x)$, can be regarded as a first successful step towards modeling of particulate charging processes in sheath/presheath regions of electronegative gases. Further models should include balance of electrons, positive/negative ions, and radicals in a discharge, ion/radical residence time, neutral drag force, as well as self-consistent equations for the sheath/presheath potential distribution.

VII. CONCLUSION

The charging and trapping of micron- and submicron-size particulates in the near-electrode regions of RF discharge in C_4F_8+Ar gas mixtures has been considered. The model near-electrode region comprises electronegative and electropositive presheath regions as well as the sheath itself. The composition of ionic species in the present study is representative to quadruple mass spectrometry experiments in low-pressure RF inductively coupled and microwave surface-wave sustained plasmas of 10% C_4F_8+90% Ar gas mixtures.[3]

It is shown that the equilibrium particulate charge in the electronegative region is lower than would be in negative-ion free plasmas, and increases towards the electrode. Near the

electrode the ion number density diminishes, and so does the dust charge. The collection of negative fluorine ions by the macroparticles has proven to be negligible. However, the effect of negative ions on dust charging and trapping is still feasible and comes into play through modification of the sheath/presheath structure. The dynamics of particulates in nearly the whole near-electrode area is controlled by competition of the electrostatic and ion drag force, whereas other forces are significant only in the electronegative plasma bulk.

Finally, we note that the sheath/presheath structure, ion fluxes, and, hence, the particulate charging and trapping processes, are very sensitive to the temperatures of electrons, positive and negative ions, as well to the electron energy distribution functions, which often appears to be bi-Maxwellian in fluorocarbon etching experiments.[3,28] The investigation of this problem is outside the scope of this work and the results will be reported elsewhere.

ACKNOWLEDGMENTS

Fruitful discussions with N. F. Cramer, S. V. Vladimirov, N. Prior, Yu. Chutov, H. Toyoda, K. Nakamura, and T. Ishijima are kindly appreciated.

This work was supported by the Japan Society for the Promotion of Science, Australian Research Council, Toshiba Corp., Nissin Inc., and Grant-in-Aid for Scientific Research from the Ministry of Education, Science, Sports, and Culture.

[1] *Plasma Etching: An Introduction*, edited by D. M. Manos and D. L. Flamm (Academic, New York, 1989).
[2] H. Sugai, K. Nakamura, T. H. Ahn, and M. Nakamura, Mater. Res. Soc. Symp. Proc. **406**, 15 (1996).
[3] H. Kokura, S. Yoneda, K. Nakamura, N. Mitsuhira, M. Nakamura, and H. Sugai, Jpn. J. Appl. Phys., Part 1 **38**, 5256 (1999).
[4] A. Kono and K. Kato, Appl. Phys. Lett. **77**, 495 (2000).
[5] K. Takahashi and K. Tashibana, J. Appl. Phys. **89**, 893 (2001).
[6] G. Selwyn, J. Singh, and R. Bennet, J. Vac. Sci. Technol. A **7**, 2758 (1989).
[7] L. Boufendi and A. Bouchoule, Plasma Sources Sci. Technol. **3**, 262 (1994).
[8] Y. Watanabe and M. Shiratani, Plasma Sources Sci. Technol. **3**, 286 (1994).
[9] *Topical Issue on the Formation, Transport and Consequencies of Particles in Plasmas*, Plasma Sources Sci. Technol. Vol. 3, No. 3 (1994).
[10] J. X. Ma and M. Y. Yu, Phys. Rev. E **50**, R2431 (1994).
[11] J. X. Ma, J. Liu, and M. Y. Yu, Phys. Rev. E **55**, 4627 (1997).
[12] K. N. Ostrikov, S. Kumar, and H. Sugai, J. Appl. Phys. **89**, 5919 (2001).
[13] T. Akimoto, E. Ikawa, T. Sango, K. Komachi, K. Katayama, and T. Ebata, Jpn. J. Appl. Phys., Part 1 **33**, 7037 (1994).
[14] H. Sugai, K. Nakamura, T. H. Ahn, and M. Nakamura, Mater. Res. Soc. Symp. Proc. **406**, 15 (1996).
[15] C. Q. Jiao, A. Garscadden, and P. D. Haaland, Chem. Phys. Lett. **297**, 121 (1998).
[16] K. Teii, M. Hori, M. Ito, T. Goto, and N. Ishii, J. Vac. Sci. Technol. A **18**, 1 (2000).
[17] F. F. Chen, *Introduction to Plasma Physics and Controlled Fusion*, 2 ed. (Plenum, New York, 1984).
[18] C. Arnas, M. Mikikian, G. Bachet, and F. Doveil, Phys. Plasmas **7**, 4418 (2000).
[19] E. A. Eidelberg and E. S. Aydil, J. Appl. Phys. **86**, 4799 (1999).
[20] L. A. Vainstein, I. I. Sobelman, and E. A. Yukov, *Atom Excitation and Spectral Line Broadening* (Nauka, Moscow, 1979).
[21] M. A. Lieberman and A. J. Lichtenberg, *Principles of Plasma Discharges and Materials Processing* (Wiley, New York, 1994), Chap. 6.
[22] A. J. Lichtenberg, V. Vahedi, M. A. Lieberman, and T. Rognlien, J. Appl. Phys. **75**, 2339 (1994).
[23] M. S. Barnes, J. H. Keller, J. C. Forster, J. O'Neill, and D. K. Coultas, Phys. Rev. Lett. **68**, 313 (1992).
[24] K. N. Ostrikov, S. V. Vladimirov, M. Y. Yu, and G. E. Morfill, Phys. Rev. E **61**, 4315 (2000).
[25] S. V. Vladimirov and N. F. Cramer, Phys. Rev. E **62**, 2754 (2000).
[26] D. Samsonov and J. Goree, Phys. Rev. E **59**, 1047 (1999).
[27] S. Xu, K. N. Ostrikov, W. Luo, and S. Lee, J. Vac. Sci. Technol. A **18**, 2185 (2000); K. N. Ostrikov, S. Xu, and M. Y. Yu, J. Appl. Phys. **88**, 2268 (2000).
[28] H. Kokura and H. Sugai, Jpn. J. Appl. Phys., Part 1 **39**, 2847 (2000).